第 35 卷第 9 期
2019 年 9 月

无 机 化 学 学 报
CHINESE JOURNAL OF INORGANIC CHEMISTRY

Vol.35 No.9
1687-1697

三羟基咔咯及其镓配合物与 DNA 的相互作用、光断裂和光动力抗肿瘤活性

陈 璇[1] 汪华华[1] Waseem Akram[1] 孙艳梅[1] 廖玉辉[2] 司利平*,[3] 刘海洋*,[1] 张启光[4]

([1]华南理工大学化学系,广东省功能分子工程重点实验室,广州 510641)

([2]南方医科大学皮肤病医院分子诊疗中心,广州 510091)

([3]佛山科学技术学院材料科学与能源工程学院,佛山 528000)

([4]Department of Chemistry, Michigan State University, E. Lansing, MI 48824, USA)

摘要:合成了一个三羟基咔咯 10-(4-羟基苯基)-5,15-双(4-(2-羟乙基)氨基-2,3,5,6-四氟苯基)咔咯(**1**)及其镓配合物(**1**-Ga)。光谱滴定实验、粘度测试和分子对接模拟结果表明,**1** 和 **1**-Ga 通过外部结合模式与小牛胸腺 DNA 发生相互作用。琼脂糖凝胶电泳实验结果表明 **1** 和 **1**-Ga 显示出良好的光核酸酶活性。2 种化合物对 A549,HepG2,MCF-7 肿瘤细胞有显著的光毒性。光辐照后,它们能通过活性氧物种(ROS)介导的线粒体途径诱导 HepG2 细胞凋亡。此外,**1**-Ga 能使肿瘤细胞周期阻滞在 G2/M 期。

关键词:咔咯;镓;DNA 断裂;光动力治疗;抗肿瘤活性

中图分类号:O614.37+1 **文献标识码**:A **文章编号**:1001-4861(2019)09-1687-11

DOI:10.11862/CJIC.2019.201

Tri-hydroxyl Corrole and Its Gallium(Ⅲ) Complex: DNA-Binding, Photocleavage and *in Vitro* Photodynamic Antitumor Activities

CHEN Xuan[1] WANG Hua-Hua[1] Waseem Akram[1] SUN Yan-Mei[1]

LIAO Yu-Hui[2] SI Li-Ping*,[3] LIU Hai-Yang*,[1] Chi-Kwong Chang[4]

([1]*Department of Chemistry, Key Laboratory of Functional Molecular Engineering of Guangdong Province, South China University of Technology, Guangzhou* 510641, *China*)

([2]*Molecular Diagnosis and Treatment Center for Infectious Diseases, Dermatology Hospital, Southern Medical University, Guangzhou* 510091, *China*)

([3]*School of Materials Science and Energy Engineering, Foshan University, Foshan, Guangdong* 528000, *China*)

([4]*Department of Chemistry, Michigan State University, E. Lansing, MI* 48824, *USA*)

Abstract: A new tri-hydroxyl corrole, 10-(4-hydroxyphenyl)-5,15-bis(4-(2-hydroxyethyl) amino-2,3,5,6-tetrafluorophenyl) corrole (**1**), and its gallium complex (**1**-Ga), were prepared. Interactions between these two corrole derivatives and calf thymus DNA were investigated by multiple spectroscopic methods, viscosity experiments and molecular docking simulation, which reveal that **1** and **1**-Ga interact with calf thymus DNA via outside binding mode. Agarose gel electrophoretic experimental results demonstrated that **1** and **1**-Ga exhibit excellent photonuclease activity. Both compounds demonstrated high photocytotoxic activity against human lung cancer cells A549, hepatoma cell HepG2 and human breast cancer cell MCF-7. After light irradiation, they might induce HepG2 cells apoptosis via ROS-mediated mitochondrial pathways. Furthermore, **1**-Ga could arrest the tumor cell cycle at G2/M phases.

Keywords: corrole; gallium; DNA-binding; photodynamic therapy; anti-tumor activity

收稿日期:2019-03-01。收修改稿日期:2019-06-06。

国家自然科学基金(No.21671068)资助项目。

*通信联系人。E-mail:chhyliu@scut.edu.cn,lipingsi@fosu.edu.cn;会员登记号:S06N7589M1006。

0 Introduction

Porphyrin derivatives have multiple applications in biology and medicine such as photodynamic therapy[1-2] and tumor imaging[3-4]. Some of them have even been used in clinical diagnosis[5-8]. Corrole is a member of porphyrin family macrocycles[9-10], whose potential anticancer application has greatly pushed the development of corrole-based bioinorganic chemistry[11-12]. In 2006, Chang et al. found that monohydroxyl corrole exhibited excellent photodynamic therapy activity against NPC tumor cells[13]. Gross et al. also found the cytotoxicity of sulfonic gallium corrole could be enhanced by light irradiation due to the generation of reactive oxygen species (ROS)[14]. Recently, tris (ethoxycarbonyl) gallium corrole was proved with high *in vitro* and *in vivo* photodynamic antitumor activity[15]. These observations demonstrated corrole is a kind of the promising photodynamic anticancer agents, and study on the design and synthesis of corrole-based photosensitizers has become a hot topic in current porphyrin chemistry[16]. It was found that cationic gallium pyridyl corrole could stabilize G-quadruplex DNA which is a target of antitumor medicine[17]. Thus, study on the interaction between corrole derivatives and DNA may also helpful to give more insight into their role in antitumor activity. In fact, the photonuclease activity and DNA binding property of many water-soluble corrole derivatives, including sulfonated[18-19], carboxyl[20], pyridyl[21-22], methyl benzoate corrole[23], have been documented, which shows these corroles exhibit good DNA-binding affinity and nuclease like activity under light irradiation.

Previously, we found polyhydric corrole exhibited significant photonuclease activity and photo-cytotoxicity towards tumor cells[24]. To further extend the scope of hydroxyl corrole along this line, herein we report the synthesis of a new 10-(4-hydroxyphenyl) -5,15-bis (4-(2-hydroxyethyl)-amino-2,3,5,6-tetrafluorophenyl) corrole (**1**), which bears two ethyl-hydroxyl groups and one hydroxyl group on periphery phenyl groups (Scheme 1). Its gallium complex **1**-Ga as well as their DNA binding properties, photonuclease activity and *in vitro* photo-cytotoxicity against human carcinoma cell lines were studied.

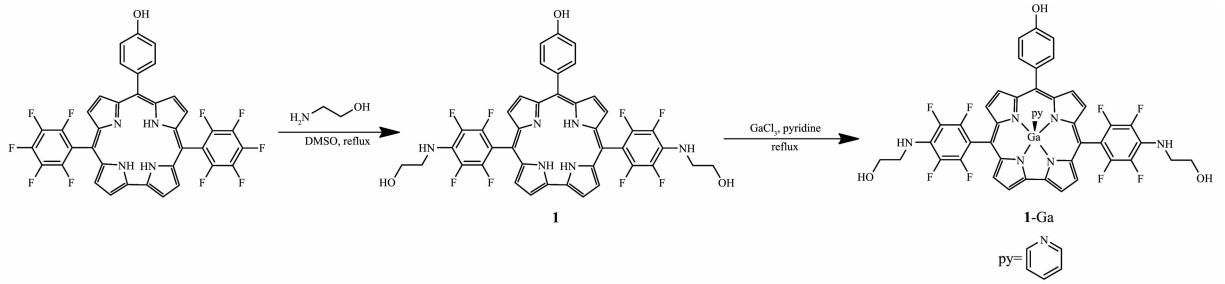

Scheme 1 Synthetic route of corrole **1** and **1**-Ga complex

1 Experimental

1.1 Chemicals and measurements

10-(4-hydroxylphenyl)-5,15-bis(pentafluorophenyl) corrole was prepared by the reported method[13]. Calf thymus DNA (CT-DNA) and Supercoiled (SC) pBR322 DNA were purchased from Sigma-Aldrich. Dimethyl sulfoxide (DMSO), tris (hydroxymethyl) aminomethane (Tris), ethidium bromide (EB), *N*,*N*-dimethylformamide (DMF), boric acid (H_3BO_3), superoxide dismutase (SOD), ethylenediaminetetraacetic acid (EDTA) and sodium chloride were supplied by Shanghai Sangon Company. Thiazolyl blue tetrazolium bromide (MTT) and 9,10-diphenylanthracene (DPA) were supplied by Adamas Reagent Company. Annexin V-FITC Apoptosis Detection Kit (C1062), cell cycle and apoptosis analysis kit (C1052), JC-1 (C2006), DAPI(C1002) and DCFH-DA (S0033) kits were obtained from Beyotime Biotechnology. Buffer Ⅰ solution (pH=7.2): containing 5 mmol·L^{-1} Tris-HCl and 50 mmol·L^{-1} NaCl; buffer Ⅱ solution (pH=7.2): containing 50 mmol·L^{-1} Tris-HCl and 18 mmol·L^{-1} NaCl; buffer Ⅲ solution (pH=8.3): containing 89 mmol·L^{-1} Tris, 89 mmol·L^{-1} H_3BO_3 and 20 mmol·L^{-1} EDTA. All solutions for biological assays

were prepared by using Ultrapure water and LED lamp (650 nm, DB-E27-5W, Likaijin) was used as light sources. MCF-7, HepG2 and A549 tumor cells were supplied by the American Type Culture Collection.

^{1}H, ^{19}F and ^{13}C NMR spectrograms were obtained in DMSO-d_6 solvent by a Bruker DRX-400 spectrometer. HR-MS spectra were obtained by VG ZAB-HS mass spectrometer. Hitachi 3900H UV-Vis spectrometer, Perkin-Elmer LS55 fluorescence Spectrophotometer and Jasco-J810 spectrometer were used in electronic spectroscopy, fluorescence quenching, and circular dichroism spectroscopy studies, respectively. Viscosity test was carried out by Ubbelohde viscometer. DYCP-31CN electrophoresis cell and Gel Doc XR system were used for Gel electrophoresis testing. Tumor cells were visualized by a TE2000-E inverted fluorescence microscope.

1.2 Synthetic methods

1.2.1 Synthesis of corrole **1**

A mixture of 10-(4-hydroxylphenyl)-5,15-bis (pentafluorophenyl) corrole (72 mg, 0.1 mmol) and 2-aminoethanol (400 μL, 6.7 mmol) in 15 mL DMSO solvent was refluxed for 2 h. After cooling down to room temperature, 50 mL CH_2Cl_2 was added. Then, the mixture was washed with saturated salt water for three times to remove DMSO and excessive ethanolamine, the organic phase was collected and dried with anhydrous sodium sulfate. After filtration, CH_2Cl_2 was removed by rotatable evaporation to afford crude product. The purple product corrole **1** was obtained by silica gel chromatography with CH_2Cl_2/CH_3OH (100∶3, *V*/*V*) mixture as eluent. Yield: 79.0%. UV-Vis (CH_2Cl_2), λ_{max}/nm (ε/(L·mol^{-1}·cm^{-1})): 417 (9.77×10^5), 569 (1.51×10^5), 616 (1.05×10^5). ^{1}H NMR (400 MHz, DMSO-d_6): δ 9.12 (s, 2H), 8.81 (s, 2H), 8.56 (s, 4H), 7.93 (d, *J*=7.5 Hz, 2H), 7.19 (d, *J*=7.4 Hz, 2H), 6.21 (s, 2H), 4.94 (s, 2H), 3.77 (s, 4H), 3.65 (s, 4H). ^{19}F NMR (376 MHz, DMSO-d_6): δ −143.08 (d, *J*=18.0 Hz), −160.43 (d, *J*=18.2 Hz). ^{13}C NMR (151 MHz, DMSO-d_6): δ 157.01 (C29), 146.77 (C9, C11), 145.19 (C6, C14), 137.51 (C21, C25, C27, C31, C33, C37), 135.94 (C22, C24, C28, C30, C34, C36), 135.34 (C1, C4, C16, C19), 132.18 (C7, C13), 129.17 (C3, C8, C12, C17), 116.41 (C2, C18), 114.21 (C20, C26, C32), 111.91 (C23, C35), 103.86 (C5, C15, C10), 60.82 (C_{NH}), 47.35 (C_{OH})(Supporting Information, Fig.S4). Elemental Anal. Calcd. for $C_{41}H_{28}F_8N_6O_3$(%): C, 61.20; H, 3.51; N, 10.44. Found(%): C, 61.17; H, 3.49; N, 10.40. HR-MS m/z: Calcd. for $C_{41}H_{29}F_8N_6O_3$([M+H]$^+$): 805.217 3, Found: 805.216 8.

1.2.3 Synthesis of **1**-Ga

Under argon atmosphere, corrole **1** (40 mg, 0.1 mmol) and dry $GaCl_3$ (100 mg, 0.6 mmol) were dissolved in 15 mL pyridine and refluxed for 1.5 h. After cooling to room temperature, 50 mL CH_2Cl_2 was added to the reaction mixture. The reaction mixture was washed more than five times with saturated salt water. Then the organic phase was collected and CH_2Cl_2 was removed by rotatable evaporation to afford crude product. Final product was obtained by silica gel chromatography with CH_2Cl_2/CH_3OH/pyridine (100∶7∶0.5; *V*/*V*) as eluents. Yield: 85%. UV-Vis (CH_2Cl_2), λ_{max}/nm (ε/(L·mol^{-1}·cm^{-1})): 422 (9.55×10^5), 534 (3.72×10^4), 574 (8.32×10^4), 608 (1.70×10^5). ^{1}H NMR (400 MHz, DMSO-d_6): δ 9.78 (s, 1H), 9.24 (d, *J*=3.7 Hz, 2H), 8.87 (d, *J*=4.1 Hz, 2H), 8.77 (s, 2H), 8.68 (d, *J*=4.5 Hz, 2H), 8.55 (d, *J*=4.2 Hz, 2H), 7.94 (d, *J*=8.0 Hz, 2H), 7.78 (t, *J*=7.6 Hz, 1H), 7.38 (dd, *J*=7.4, 5.6 Hz, 2H), 7.18 (d, *J*=8.1 Hz, 2H), 6.08 (s, 2H), 4.97 (t, *J*=5.3 Hz, 2H), 3.78 (dd, *J*=11.5, 5.8 Hz, 4H), 3.64 (d, *J*=5.9 Hz, 4H). ^{19}F NMR (376 MHz, DMSO-d_6): δ −142.06 (s), −160.49 (s). ^{13}C NMR (151 MHz, DMSO-d_6): δ 156.64 (C29), 149.50 ($C_{pyridine\text{-}o}$), 143.71 (C9, C11), 141.08 (C6, C14), 137.07 ($C_{pyridine\text{-}p}$), 136.08 (C21, C25, C27, C31, C33, C37), 134.92 (C22, C24, C28, C30, C34, C36), 133.91 (C1, C4, C16, C19), 132.35 (C7, C13), 129.60 (C3, C8, C12, C17), 123.85 ($C_{pyridine\text{-}m}$), 116.34 (C2, C18), 114.09 (C20, C26, C3), 110.87 (C23, C35), 98.01 (C5, C15, C10), 60.75 (C_{NH}), 47.44 (C_{OH})(Fig.S8). Elemental Aanal. Calcd. for $C_{46}H_{30}F_8N_7O_3Ga$(%): C, 58.13; H, 3.18; N, 10.32. Found(%): C, 58.09; H, 3.14; N, 10.29. HR-MS *m*/*z*: Calcd. for $C_{41}H_{25}F_8N_6O_3Ga$ ([M−Py]$^+$): 870.111 6, Found: 870.111 1.

1.3 Absorption spectroscopic assay

In electronic absorption titration assay, we kept the concentrations of compounds constant and record the absorption values after continuous addition of 2

μL CT-DNA (1.5 mmol·L^{-1}). The intrinsic binding constant (K_b) of the compound is determined by following equation[25]:

$$\frac{c_{DNA}}{\varepsilon_a-\varepsilon_f}=\frac{c_{DNA}}{\varepsilon_b-\varepsilon_f}+\frac{1}{K_b(\varepsilon_b-\varepsilon_f)} \quad (1)$$

where ε_f and ε_b are extinction coefficient of the compound when incompletely and completely bind to DNA respectively; ε_a is the extinction coefficient of the compound in the presence of DNA, and c_{DNA} is the concentration of DNA. By graphing the plot of $c_{DNA}/|\varepsilon_a-\varepsilon_f|$ versus c_{DNA}, K_b might be calculated by y-intercept.

1.4 Fluorescence titration assay

A solution (3 mL) containing 30 μmol·L^{-1} CT-DNA and 5 μmol·L^{-1} EB in buffer Ⅰ solutions was titrated with increasing the amount of compound and measured after incubated for 3 min. The quenching constants (K_{SV}) is obtained by the following Stern-Volmer equation[26]:

$$F_0/F=1+K_{SV}c_{compound} \quad (2)$$

where $c_{compound}$ is the concentration of compound, F_0 and F are the fluorescence intensities in the absence and presence of the compound, respectively.

1.5 Circular dichroism spectral studies

CD spectra were recorded with polarimeter by using a 1 cm quartz cell with scanning wavelength number from 600 to 200 nm. We kept CT-DNA at a constant concentration and added the compounds with suitable concentrations, and all CD spectra were recorded three times and background was automatically subtracted.

1.6 Viscosity studies

Viscosity test was conducted by Ubbelohde viscometer in a thermostatic (30.0 ℃±0.1 ℃) water bath. The flow times were recorded by digital stopwatch with the concentration of the compound increasing, which was taken the average value of five times. The result was presented as $(\eta/\eta_0)^{1/3}$ vs $c_{compound}/c_{DNA}$, where η and η_0 are the relative viscosity of CT-DNA in the presence and absence of the compound, respectively. Specific viscosity is evaluated by the equation[27]:

$$\eta=(t-t_0)/t_0 \quad (3)$$

Where t_0 and t are the flow time of CT-DNA in the absence and presence of the compound, respectively.

1.7 Molecular docking studies

AutoDock Tools (ADT) v1.5.6 was used to perform molecular docking. The DNA (d(CGCGAATTCGCG)2) structure data was got from the Protein Data Bank (PDB ID: 1BNA). The geometry of corrole derivatives was optimized with Gaussian 09. The DNA duplex was enclosed in grid dimensions (6 nm×6 nm×6 nm) and a grid spacing of 0.037 5 nm. Kollman method incorporated in AutoDock software was used for docking calculations. The lowest energy docked conformation was chosen as the binding mode[28].

1.8 DNA cleavage assay

The photocleavage activity assay was performed by using agarose gel electrophoresis. The reaction mixtures were in a total volume of 10 μL, containing supercoiled pBR322 DNA (0.1 μg) and different concentrations of complexes in buffer Ⅱ (10% DMF). Then the mixture was put under the filament lamp and irradiated for 2 h. After staining with an EB dilute solution, DNA bands were captured by using Gel Doc XR system. The photocleavage mechanistic studies were performed by using multiple reactive oxygen species scavengers.

1.9 Cytotoxic activity assays

Cells (MCF-7, HepG2, A549) in 100 μL of medium containing 10% fetal bovine serum were seeded in 96-well plates (5×10^3 cells per well) and incubated overnight in cell incubator (37 ℃ and 5%(V/V) CO_2). In the treatment of **1** and **1**-Ga, DMSO (final concentration ≤1% in the test culture) was used as a solvent to prepare different concentrations of the drug and diluted with the cell culture medium. There were 5 multiple pores in each group. After incubation for 2 hours and irradiation treatment by red light for 1 hour, cells were further incubated for 48 hours. Removed the medium with drugs, 100 μL of MTT containing medium (250 μg·mL^{-1}) was then added to each well carefully. The cells were incubated for three hours, optical density (OD) value were calculated by using a microplate spectrophotometer at 490 nm. The IC_{50} value was obtained by Graph Pad Prism 7.0 software and represents the mean of five independent experiments.

1.10 Reactive oxygen species (ROS) detection in cells

HepG2 cells suspended in 2 mL of culture medium were seeded in 6-well plates (1×10^5 cells per well) and cultured overnight in cell incubator. Then the cells were incubated with **1** (0.1 μmol·L^{-1}) and **1**-Ga (5 μmol·L^{-1}) and treated with the same illumination condition as previously described above. After cultured cells for 24 h, the medium was removed. According to the instruction of test kit, cells were stimulated with suitable concentration of DCHF-DA for 30 min under the dark. The fluorescence image acquisitions were performed by fluorescence microscope.

1.11 Mitochondrial transmembrane potential analysis

HepG2 cells suspended in 2 mL of culture medium were plated into 6-well plates (1×10^5 cellsperwell) and cultured overnight under dark. Then the cells were incubated with **1** (0.1 μmol·L^{-1}) and **1**-Ga (5 μmol·L^{-1}) and irradiated with the same illumination condition as previously described above. After being treated by using JC-1 kits and washed with PBS buffers more than three times, cells photos were obtained by using TE2000-E inverted fluorescence microscope.

1.12 Flow cytometry analysis

HepG2 cells were seeded into 6-well plates (1×10^6 cells per well) and incubated overnight. The cells were incubated with **1** (0.1 μmol·L^{-1}) and **1**-Ga (5 μmol·L^{-1}) and irradiated with the same illumination condition as described above. Adherent cells were washed and dealt with pancreatin. According to the manufacturers operating instruction, cells were incubated with Annexin V-FITC after re-suspended and centrifuged. The cell cycle assay was performed by propidium staining. Data acquisition and analysis were implemented by a FACS Calibur flow cytometer and FlowJo10.0 Software respectively.

2 Results and discussion

2.1 DNA interaction and photocleavage

The UV-Vis spectra titration is one of simplest techniques for detecting DNA binding mode. Intercalation binding will cause a significant red shift and a large hypochromic effect, while external binding brings a slight red shift and a smaller hypochromic effect in the spectra[29]. As shown in Fig.1, with the addition of DNA, only small hypochromic and bathochromic shift of the spectra could be observed. This suggested an outside binding mode between these corroles and CT-DNA[18,30]. The intrinsic binding constants K_b for **1**-Ga and **1** are 1.69×10^5 and 1.13×10^5 L·mol^{-1}, respectively. **1** and **1**-Ga showed the same binding affinity to CT-DNA. Spectroscopic titration data are summarized in Table 1.

EB shows weak fluorescence in buffer solution, but exhibits strong fluorescence after inserting into the base pair of DNA[31]. Thus, EB is often used as the fluorescence probe to detect the interaction between small molecules and DNA. Fig.2 is the fluorescence

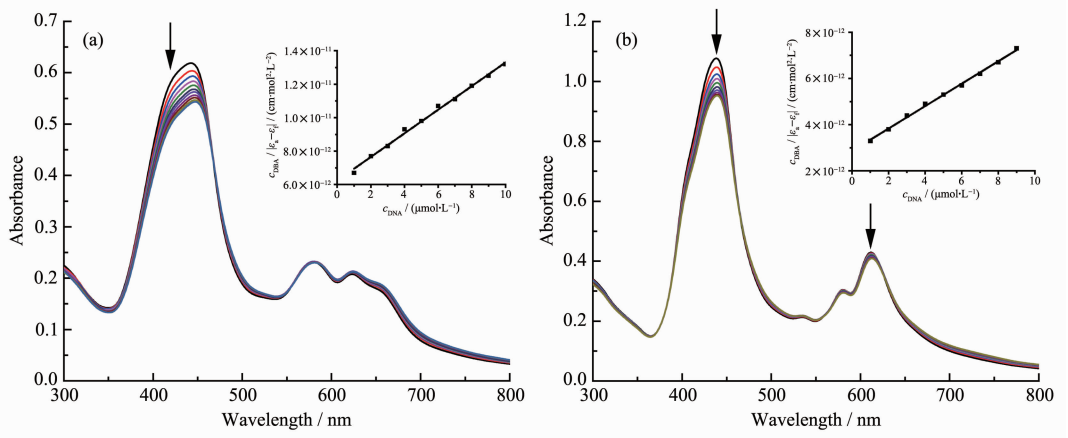

Inset: plot of $c_{DNA}/|\varepsilon_a-\varepsilon_f|$ vs c_{DNA}

Fig.1　UV-Vis spectra changes of 10 μmol·L^{-1} **1** (a) and **1**-Ga (b) with increasing concentration of CT-DNA

Table 1 Spectroscopic titration data of corrole 1 and 1-Ga binding with CT-DNA

Complex	Red shift / nm	Hypochromicity / %	K_b / (L·mol^{-1})	K_{SV} / (L·mol^{-1})
1	2	2.4	1.13×10^5	5.6×10^4
1-Ga	1	2.7	1.69×10^5	1.03×10^5

spectra changes of EB/CT-DNA upon the addition of **1**-Ga and **1**. The EB fluorescence decreased remarkably with the increasing of the concentration of both corroles. As EB is a strong intercalator, the replacement of EB by corrole is not possible. The fluorescence quenching of the system is caused by the dynamic or static process of the interaction between the EB/CT-DNA and corroles. The Stern-Volmer quenching rate constants K_{SV} for **1** and **1**-Ga were 5.6×10^4 and 1.03×10^5 L·mol^{-1}, respectively, indicating strong interactions between CT-DNA and these corroles. The K_{SV} results are also comparable to the absorption titration assay.

CD spectra is sensitive to DNA conformation transformation during complexes-DNA interactions. The outside binding of the complex causes little variation on the base stacking and helical structure of DNA, and there are no significant changes in CD spectra could be observed. But intercalation binding mode will cause the remarkable enhancement of both CD peaks of CT-DNA[32]. CD spectral changes of CT-DNA upon the addition of **1** and **1**-Ga are shown in Fig.3. Small decrease in both CD signal intensity of CT-DNA were observed when binding **1** and **1**-Ga, excluding the intercalation interaction mode. Noteworthy, no exciton coupling CD peaks were observed in the Soret band of corrole in both cases, indicating

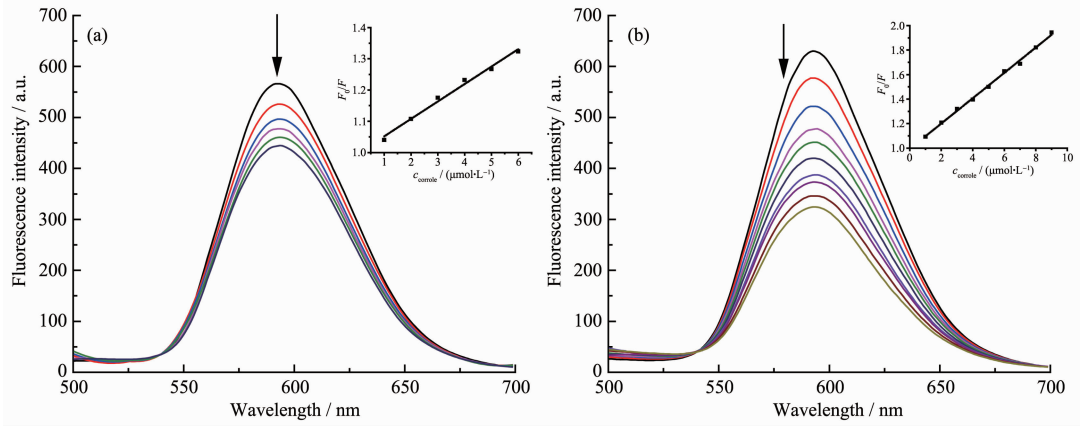

λ_{ex}: 370 nm; Inset: plot of F_0/F vs $c_{compound}$

Fig.2 Fluorescence spectra changes of EB bind to CT-DNA with increasing concentration of **1** (a) and **1**-Ga (b)

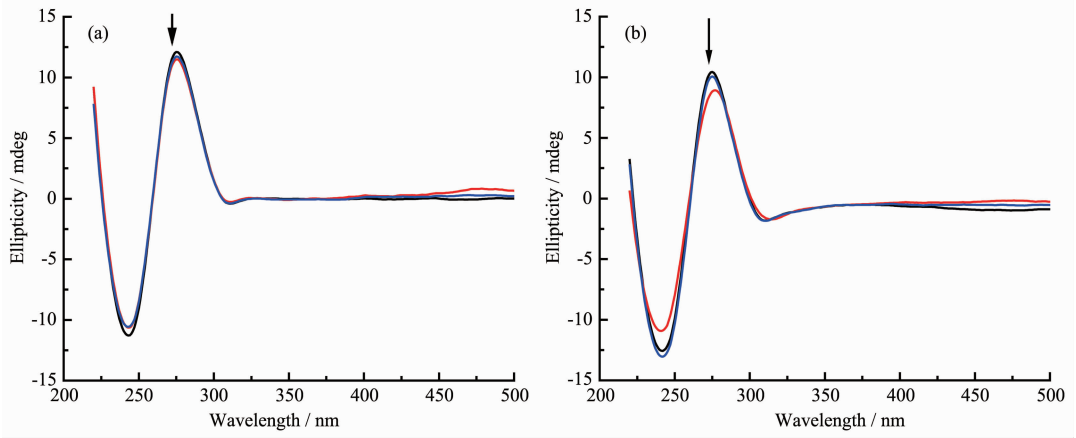

$c_{compound}/c_{DNA}$=0, 0.1, 0.2

Fig.3 CD spectra changes of 0.15 mmol·L^{-1} CT-DNA with addition of **1** (a) and **1**-Ga (b)

the outside binding corrole **1** or **1**-Ga are not ordered in a chiral manner.

Viscosity measurement is the most important method for investigating DNA binding mode in lack of crystal data. Intercalation binding will result in the viscosity increase remarkably, while outside binding has little effect on the viscosity[33]. The viscosity of CT-DNA did not change obviously with the addition of corrole indicating **1** and **1**-Ga interact with CT-DNA via an outside binding mode. This is in accordance with the spectroscopic titration results.

To further investigate the interaction between **1** and **1**-Ga and DNA, we have also performed molecular docking simulations. The energy-minimized molecular docking simulated conformation of duplex DNA and **1** or **1**-Ga are shown in Fig.5, which reveals that both corroles interact with DNA in major groove. Corrole **1** situated around DA18, DA17, DA6, DA5, DG4, DT19 and DC3 base pairs. One H-bond between amino-ethyl hydroxyl group and DG16 base. While **1**-Ga was found situated around DA18, DA17, DA6, DA5, DG3 and DG4 base pairs. Except for one H-bond between phenyl hydroxyl and DC3 base, one phenyl group was observed partially intercalated into DA5-DA6 base pair. The binding energy for **1** and **1**-Ga were −27.8 and −34.8 kJ·mol^{-1} respectively, showing **1**-Ga has higher binding affinity to DNA.

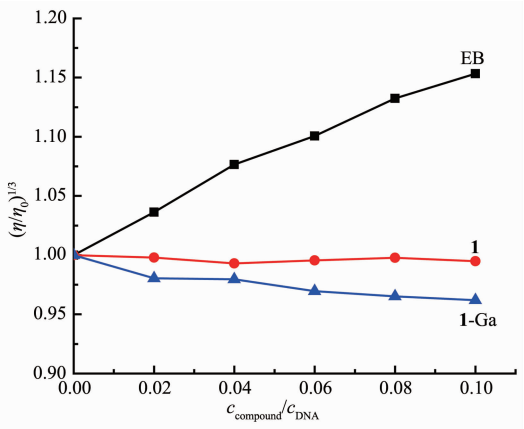

Fig.4　Effect of concentration of **1**, **1**-Ga and EB on relative viscosity of 0.1 mmol·L^{-1} CT-DNA

Many corrole complexes show photonuclease activity[24,34]. DNA photocleavage efficiency of **1** and **1**-Ga were evaluated by using pBR322 DNA. As shown in Fig.6, no cleaved plasmid DNA could be observed for control or test sample under dark condition. After light irradiation for 2 h, both **1** and **1**-Ga exhibited significant photonuclease activity and supercoiled pBR322DNA (Form Ⅰ) was transformed to nicked form (Ⅱ) with **1**-Ga showing better performance. When corrole concentration reached 160 μmol·L^{-1}, 90% and

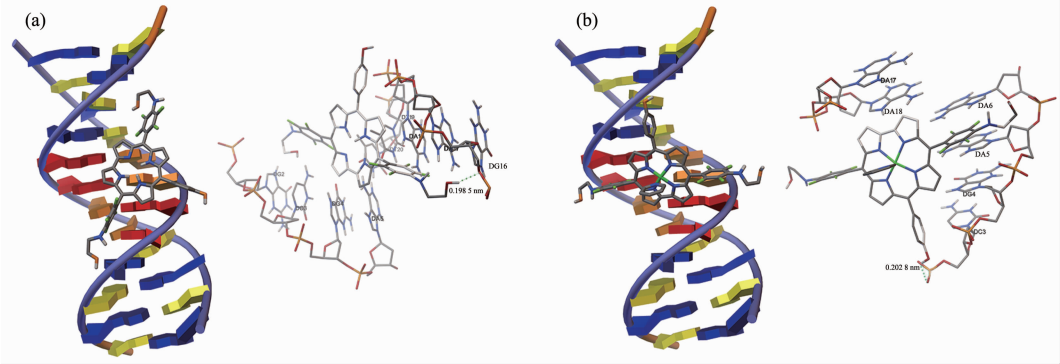

Fig.5　Molecular docked structure of **1** (a) and **1**-Ga (b) with DNA

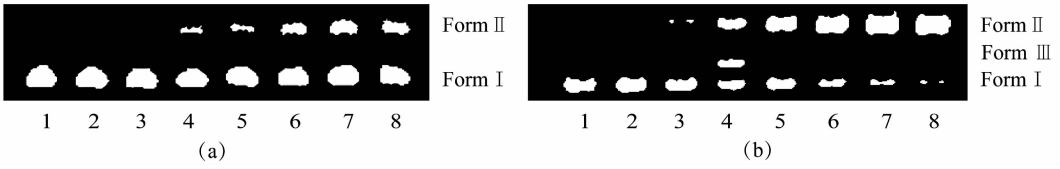

Lane 1~2: DNA control (irradiation or dark), lane 3: 40 μmol·L^{-1} corrole+DNA (dark), lane 4~8: corrole+DNA (irradiation); $c_{compound}$=20, 40, 80, 120, 160 μmol·L^{-1}

Fig.6　DNA photocleavage at different concentrations of **1** (a) and **1**-Ga (b) with 2 h irradiation

50% supercoiled pBR322DNA was transformed to nicked form Ⅱ for **1**-Ga and **1**, respectively. Interestingly, form Ⅲ DNA was observed for **1**-Ga when its concentration was 20 μmol·L^{-1} (Fig.6b, lane 4).

To check the reactive oxygen species (ROS) involved in DNA photo-cleavage by corrole, inhibitation tests were carried out by using different oxidant inhibitors (Fig.7). The reagent NaN_3 (lane 4) is the scavengers of singlet oxygen ($^1O_2$), KI (lane 5) is the scavenger of hydroxyl radical (·OH) and SOD (lane 6) is the scavenger of superoxide anion radical ($\cdot O_2^-$). NaN_3 inhibitor could remarkably inhibit the DNA cleavage by **1**, indicating singlet oxygen was the main ROS involved. While for **1**-Ga, both NaN_3 and KI were observed to inhibit the DNA cleavage obviously. This suggests singlet oxygen and hydroxyl radical are involved in **1**-Ga. SOD had small inhibition effect to DNA cleavage by **1** and no effect to the DNA cleavage by **1**-Ga.

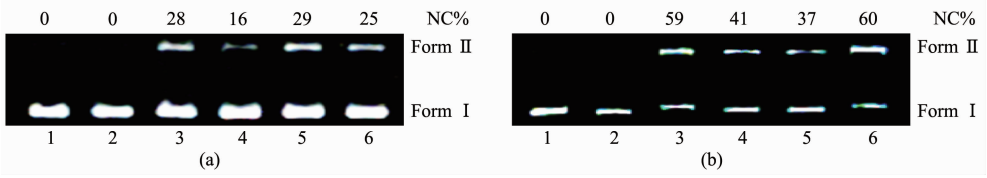

Lane 1~2: DNA control (irradiation or dark), lane 3: corrole+DNA, lane 4: corrole+DNA+10 μmol·L^{-1} NaN_3, lane 5: corrole+DNA+50 μmol·L^{-1} KI, lane 6: corrole+DNA+1000 U·mL^{-1} SOD

Fig.7 DNA photocleavage in the presence of oxidant inhibitors: (a), 20 μmol·L^{-1} **1**; (b) 20 μmol·L^{-1} **1**-Ga after irradiation for 2 h

2.2 Photodynamic antitumor activity cytotoxicity

The cytotoxicity of **1** and **1**-Ga was evaluated by MTT method by using three tumor cell lines MCF-7 (breast), HepG2 (liver) and A549 (lung). Temoporfin (mTHPC, the second generation PDT clinical drug) was used as the control under the same experimental conditions. The IC_{50}[35] of **1** and **1**-Ga were calculated by graphing analysis of dose-response curves and summarized in Table 3. Both **1** and **1**-Ga exhibited excellent photocytotoxicity to all tested tumor cell lines. Especially, **1** showed better PDT performance than mTHPC, indicating it is a promising candidate for PDT drug. For HepG2 and A549 tumor cell, **1**-Ga exhibited significant lower photocytotoxcity than **1**. Their dark cytotoxicity is around three times stronger than mTHPC and **1**-Ga displayed higher dark cytotoxicity than **1**. It could be observed that MCF-7 was much sensitive to **1**-Ga than HepG2 and A549 tumor cells.

The generation of ROS, especially singlet oxygen, is closely related to the cell death in PDT treatment. Here, fluorescence microscope was used to detect the cellular ROS level changes. 2′,7′-dichlorodihydrofluorescein diacetate (DCFH-DA) and Rosup was used as a fluorescent dye and positive control respectively. DCFH-DA is a non-fluorescent dye, which could be oxidized to the fluorescent compound DCF with green fluorescence. Fig.8 shows qualitative detection of ROS generation in HepG2 cells. Green emission was observed after PDT treatment by **1** and **1**-Ga, showing that cellular ROS level increased. This imply the photocytotoxicity of **1** and **1**-Ga may relate to the oxidative stress reaction of the tumor cells.

The destruction in mitochondrial membrane

Table 2 IC_{50} values of corroles against tumor cells

μmol·L^{-1}

Complex	MCF-7		HepG2		A549	
	dark	light	dark	light	dark	light
1	73.0±8.4	0.3±0.1	51.5±6.8	<0.1	>150	0.3±0.1
1-Ga	42.5±5.5	<0.1	43.4±7.7	4.1±0.1	30.2±0.1	4.9±0.3
mTHPC	177.1±19.5	1.1±0.3	129±16.2	1.3±0.5	141.6±19.7	0.5±0.2

potential (MMP) is related to cytochrome c triggered cell apoptosis[36]. MMP changes may be monitored by using the JC-1 fluorescent dye. JC-1 forms aggregates and emit red fluorescence in the normal mitochondrial matrix. It will be in its monomer form and emit green fluorescence when the MMP decreases. Carbonyl cyanide 3-chlorophenylhydrazone (CCCP) could promote the permeability of mitochondrial inner membrane to H^+ and destruct the MMP. Here, CCCP is used as the positive control for MMP detection. As shown in Fig.9, green fluorescence could be observed after PDT treatment with **1** and **1**-Ga, which is similar to the treatment by CCCP. This indicates the PDT treatment by **1** and **1**-Ga causes MMP destruction, which may further trigger tumor cell apoptosis.

Fig.10 shows the flow cytometry diagram double

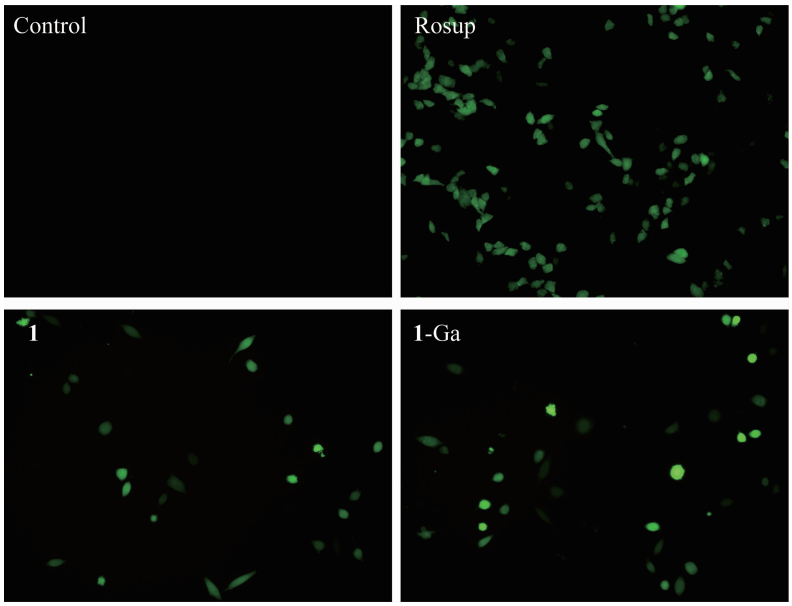

Fig.8　Effect of **1** (0.1 μmol·L^{-1}) and **1**-Ga (5 μmol·L^{-1}) PDT treatment on the intracellular ROS in HepG2 cells with DCHF-DA as fluorescence probe at 200× magnification

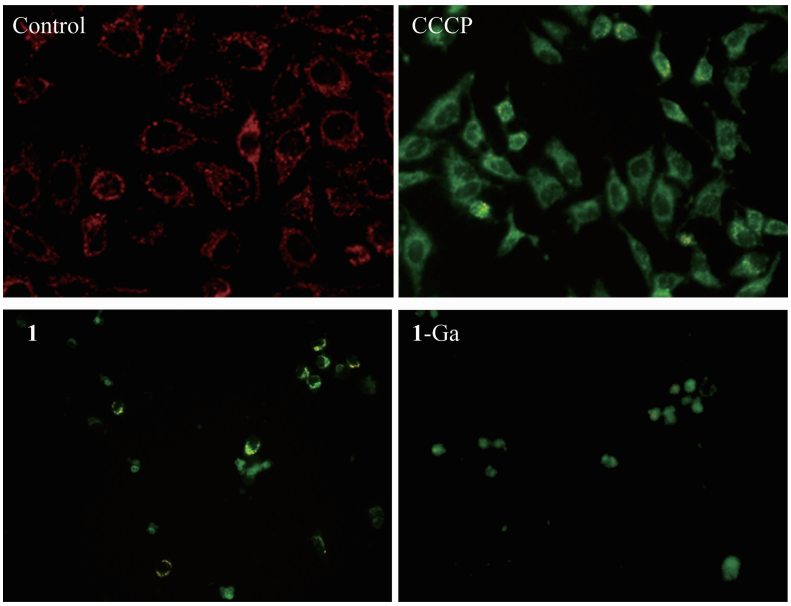

Fluorescence probe: JC-1; Positive control: CCCP dye

Fig.9　Effect of PDT treatment by **1** (0.1 μmol·L^{-1}) and **1**-Ga (5 μmol·L^{-1}) on mitochondrial transmembrane potential of HepG2 cells at 200× magnification

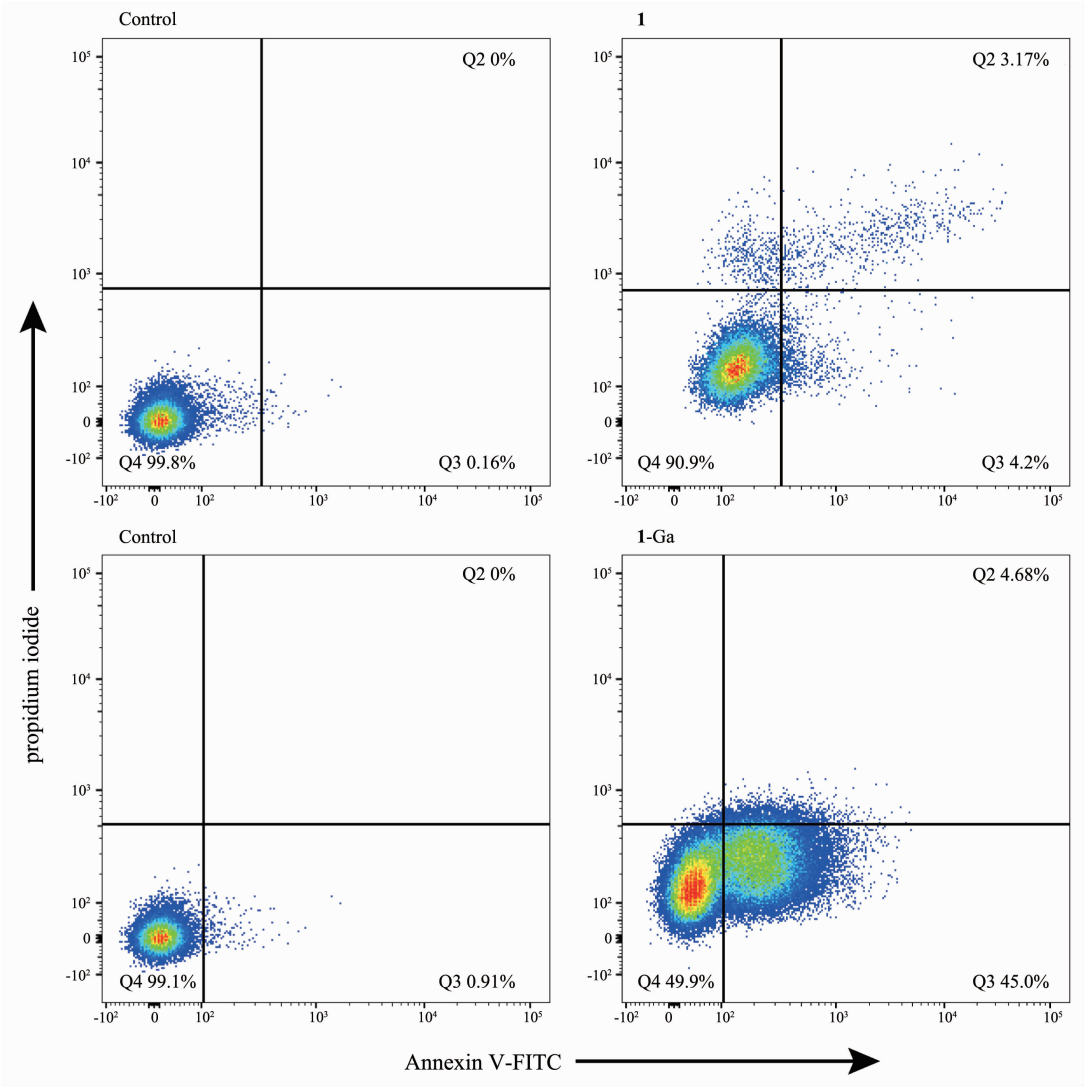

Cells were double labeled by annexin V and PI

Fig.10 Flow cytometric diagram of HepG2 cells after PDT treatment by 0.1 μmol·L^{-1} of **1** and 2 μmol·L^{-1} of **1**-Ga

labeled by FITC and PI fluorescence dyes. Quadrant 2, 3 and 4 are assigned as late-stage apoptotic cells, early-stage apoptotic cells and living cells, respectively. Significantly, late- or early-stage apoptotic tumor cells could be observed after PDT treatment by **1** or **1**-Ga, suggesting the tumor cells die via apoptotic pathway.

The regulation of cell death is also related to alterations of cell cycle. Tumor cell cycle arrest means the block of DNA synthesis. The cell cycle distribution may be easily checked with flow cytometry by using propidium iodide (PI) fluorescence probe. The cell cycle distribution is shown in Fig.11. After PDT treatment, **1**-Ga could remarkably arrest the cell cycle at G2/M phase and **1** exhibited little effect to the cell cycle distribution.

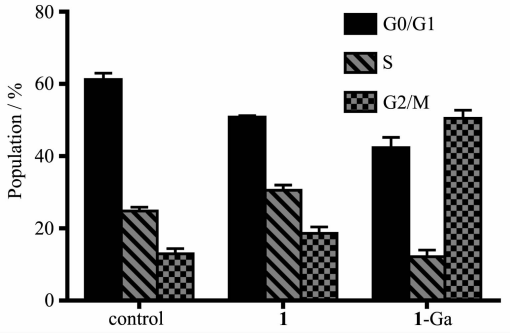

Fig.11 Cell cycle distribution of HepG2 cells after PDT treatment

3 Conclusions

In summary, a new hydroxyl corrole **1** and its

metal complex **1**-Ga had been synthesized. Both **1** and **1**-Ga complex interact with CT-DNA via outside binding mode. **1**-Ga displays higher DNA binding affinity than **1**, which is also supported by molecular docking binding energy. Both **1** and **1**-Ga could cleave supercoiled pBR322 DNA efficiently after irradiation. Singlet oxygen ($^1O_2$) is the main active oxidant for **1**, while singlet oxygen and hydroxyl radical are involved for **1**-Ga photonuclease activity. Furthermore, **1** and **1**-Ga exhibit strong photocytotoxic toward breast, hepatoma, and lung cancer cells. After PDT treatment, **1**-Ga can induce cell cycle arrest at G2/M phase. The present observation suggests that corrole PDT treatment will promote the cellular ROS level, destruct the mitochondrial transmembrane potential and finally induce the tumor cell apoptosis. Investigation on the detailed signaling pathway of the tumor cell apoptosis is still going on in our laboratory.

Acknowledgments: This work was supported by National Natural Science Foundation of China (Grant No.21671068).

Supporting information is available at http://www.wjhxxb.cn

References:

[1] Ethirajan M, Chen Y H, Joshi P, et al. *Chem. Soc. Rev.*, **2011**,**40**(1):340-362

[2] Ferreira D P, Conceição D S, Calhelha R C, et al. *Carbohydr. Polym.*, **2016**,**151**:160-171

[3] Zhu M L, Zhang J L, Zhou Y B, et al. *Inorg. Chem.*, **2018**,**57** (18):11537-11542

[4] Josefsen L B, Boyle R W. *Theranostics*, **2012**,**2**(9):916-966

[5] Sutedja T, Baas P, Stewart F, et al. *Eur. J. Cancer*, **1992**,**28** (8/9):1370-1373

[6] Nathan T R, Whitelaw D E, Chang S C, et al. *The Journal of Urology*, **2002**,**168**(4):1427-1432

[7] Chang S C, Buonaccorsi G A, MacRobert A J, et al. *Prostate*, **1999**,**32**(2):89-98

[8] Hsi R A, Kapatkin A, Strandberg J, et al. *Clin. Cancer Res.*, **2001**,**7**(3):651-660

[9] Kadish K M, Smith K M, Guilard R. *The Porphyrin Handbook*: *Vol.*33. San Diego: Academic Press, **2000**:201-232

[10]Gryko D T, Fox J P, Goldberg D P. *J. Porphyrins Phthalocyanines*, **2004**,**8**(9):1091-1105

[11]Aviv-Harel I, Gross Z. *Chem. Eur. J.*, **2009**,**15** (34):8382-8394

[12]Driggers E M, Hale S P, Lee J B, et al. *Nat. Rev. Drug Discovery*, **2008**,**7**:608-624

[13]Chang C K, Kong P W, Liu H Y, et al. *Proc. SPIE*, **2006**, **6139**:613915

[14]Hwang J Y, Lubow D J, Chu D, et al. *J. Controlled Release*, **2012**,**163**(3):368-373

[15]Zhang Z, Wang H H, Yu H J, et al. *Dalton Trans.*, **2017**,**46** (29):9481-9490

[16]Teo R D, Hwang J Y, Termini J, et al. *Chem. Rev.*, **2017**, **117**(4):2711-2729

[17]Zhang Z, Wen J Y, Lv B B, et al. *Appl. Organomet. Chem.*, **2016**,**30**(3):132-139

[18]Huang J T, Wang X L, Zhang Y, et al. *Transition Met. Chem.*, **2013**,**38**(3):283-289

[19]Zhang Y, Wen J Y, Mahmood M H, et al. *Luminescence*, **2015**,**30**(7):1045-1054

[20]Zhang Y, Wang Q, Wen J Y, et al. *Chin. J. Chem.*, **2013**,**31** (10):1321-1328

[21]Zhang Y, Wen J Y, Wang X L, et al. *Appl. Organomet. Chem.*, **2014**,**28**(7):559-566

[22]Liang Z H, Liu H Y, Zhou R, et al. *J. Membr. Biol.*, **2016**, **249**(4):419-428

[23]Wang J M, Li Y, Yuan H Q, et al. *Appl. Organomet. Chem.*, **2016**,**31**(3):e3571

[24]Liang Z H, Liu H Y, Jiang G B, et al. *Chin. J. Chem.*, **2016**, **34**(10):997-1005

[25]Wolfe A, Shimer G H, Meehan T. *Biochemistry*, **1987**,**26** (20):6392-6396

[26]Lakowicz J R, Weber G. *Biochemistry*, **1973**,**12** (21):4161-4170

[27]Cohen G, Eisenberg H. *Biopolymers*, **1969**,**8**(1):45-55

[28]Wei D G, Wilson W D, Neidle S. *J. Am. Chem. Soc.*, **2013**, **135**(4):1369-1377

[29]Pasternack R F, Gibbs E J, Villafranca J J. *Biochemistry*, **1983**,**22**(23):5409-5417

[30]Zhao P, Xu L C, Huang J W, et al. *Spectrochim. Acta Part A*, **2008**,**71**(4):1216-1223

[31]Olmsted J, Kearns D R. *Biochemistry*, **1977**,**16** (16):3647-3654

[32]Nordén B, Tjerneld F. *Biopolymers*, **1982**,**21**(9):1713-1734

[33]Satyanarayana S, Dabrowiak J C, Chaires J B. *Biochemistry*, **1993**,**32**(10):2573-2584

[34]Wang Y G, Zhang Z, Wang H, et al. *Bioorg. Chem.*, **2016**, **67**:57-63

[35]Stewart M J, Watson I D. *Br. J. Clin. Pharmacol.*, **1983**,**16** (1):3-7

[36]Hwang J Y, Lubow D J, Sims J D, et al. *J. Biomed. Opt.*, **2012**,**17**(1):015003